Electron tunneling characteristics of a cubic quantum dot, $(PbS)_{32}$

Sanjeev K. Gupta,[1,a)] Haiying He,[2,a)] Douglas Banyai,[1] Anil K. Kandalam,[3] and Ravindra Pandey[1]
[1]*Department of Physics, Michigan Technological University, Houghton, Michigan 49931, USA*
[2]*Department of Physics and Astronomy, Valparaiso University, Valparaiso, Indiana 46383, USA*
[3]*Department of Physics, West Chester University of Pennsylvania, West Chester, Pennsylvania 19383, USA*

(Received 13 August 2013; accepted 20 November 2013; published online 27 December 2013)

The electron transport properties of the cubic quantum dot, $(PbS)_{32}$, are investigated. The stability of the quantum dot has been established by recent scanning tunneling microscope experiments [B. Kiran, A. K. Kandalam, R. Rallabandi, P. Koirala, X. Li, X. Tang, Y. Wang, H. Fairbrother, G. Gantefoer, and K. Bowen, J. Chem. Phys. **136**(2), 024317 (2012)]. In spite of the noticeable energy band gap (~2 eV), a relatively high tunneling current for $(PbS)_{32}$ is predicted affirming the observed bright images for $(PbS)_{32}$. The calculated *I-V* characteristics of $(PbS)_{32}$ are predicted to be substrate-dependent; $(PbS)_{32}$ on the Au (001) exhibits the molecular diode-like behavior and the unusual negative differential resistance effect, though this is not the case with $(PbS)_{32}$ on the Au (110). Appearance of the conduction channels associated with the hybridized states of quantum dot and substrate together with their asymmetric distribution at the Fermi level seem to determine the tunneling characteristics of the system. © *2013 AIP Publishing LLC*. [http://dx.doi.org/10.1063/1.4849136]

I. INTRODUCTION

The lead-chalcogenide semiconducting quantum dots (QDs) have recently attracted a wide attention due to their stronger quantum-confinement effects than in II-VI and III-V based QDs.[1] Among the lead-chalcogenides, lead sulfide (PbS) QDs have been of a special interest due to their potential applications in IR photo-detection, photovoltaics, and solar cells.[2–12] Recently, the possibility of a single PbS nanowire (NW) based FET device has also been explored both in experiments and theoretical studies.[13,14] In a very recent experimental study, band-gap controlled PbS nanocrystals of various sizes were synthesized to study the effect of band-gap energy on the photovoltaic performance.[15] This study has shown that an optimal band-gap of 1.2 eV maximizes the photovoltaic device performance.

While polymer-conjugated, core-shell, and colloidal PbS QDs in the size-ranges of 2–10 nm have been the subject of many studies, focus on bare and ultra-small (<1 nm) PbS QDs has been rather scarce.[16–18] As to our knowledge there are no studies on the electron transport properties of ultra-small PbS QDs. In this paper, we focus on the smallest cubic QD of PbS, namely, $(PbS)_{32}$ whose structure and stability was established recently.[19] Since the structure of $(PbS)_{32}$ bears a resemblance to that of the bulk crystal, it has been termed as "baby crystal." The pattern of aggregation when $(PbS)_{32}$ deposited on a substrate was also confirmed by the images obtained by scanning tunneling microscope (STM).[19] In this paper, we now look into examining the electron transport properties of the cubic quantum dot, $(PbS)_{32}$, deposited on the Au substrate. We give details of the computational method in Sec. II. Results are discussed in Sec. III, and summary is given in Sec. IV.

a)Authors to whom correspondence should be addressed. Electronic addresses: sanjeevg@mtu.edu and haiying.he@valpo.edu

II. COMPUTATIONAL METHOD

Spin-unpolarized electronic structure calculations are carried out using the density functional theory (DFT) method as implemented in the Vienna *ab initio* simulation package (VASP).[20] The exchange and correlation effects are described using the PW91 functional form to DFT.[21] We use the Bardeen, Tersoff, and Hamann (BTH) formalism[22] of electron tunneling to calculate the tunneling current in a STM-like setup where the gold electrode is weakly coupled to the cubic quantum dot, $(PbS)_{32}$.[23]

In the low-bias limit, the electron tunneling current between two electrodes can be calculated at finite temperature as follows:[22]

$$\begin{aligned} I = \frac{4\pi e}{\hbar}\gamma \int_{-\infty}^{+\infty} \rho_s\left(\varepsilon + \frac{eV}{2}\right)\rho_t\left(\varepsilon - \frac{eV}{2}\right) \\ \times e^{-2d\sqrt{2(m/\hbar^2)(\varphi_{av}-\varepsilon)}} \\ \times \left\{\left[f\left(\varepsilon - \frac{eV}{2}\right)\right]\left[1 - \left[f\left(\varepsilon + \frac{eV}{2}\right)\right]\right] \right. \\ \left. - \left[f\left(\varepsilon + \frac{eV}{2}\right)\right]\left[1 - \left[f\left(\varepsilon - \frac{eV}{2}\right)\right]\right]\right\} d\varepsilon, \quad (1) \end{aligned}$$

where ρ_s and ρ_t are the projected densities of states (DOSs) of the sample – $(PbS)_{32}$ and the tip cap, respectively, d is the distance of the tip from $(PbS)_{32}$, ε is the injection energy of the tunneling electron, e is the electronic charge, m is the effective mass of the electron, $\hbar$ is the Planck constant, ϕ_{av} is the average work function of $(PbS)_{32}$ and the tip, and f is the Fermi distribution function. At low-bias regime, the effective mass of the electron (m) and the average work function are assumed to be constant. To match the respective electrochemical potentials at zero bias, the Fermi energy of $(PbS)_{32}$

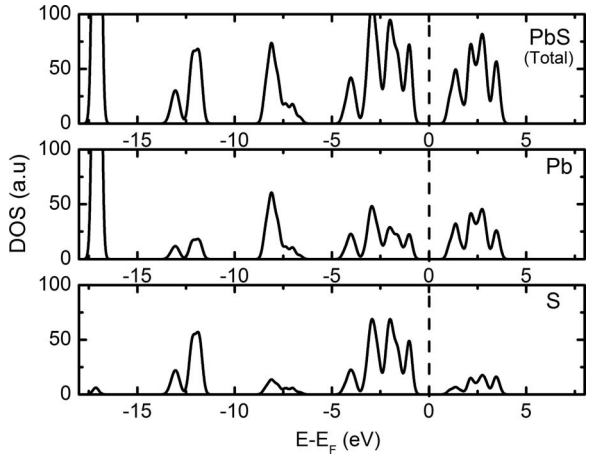

FIG. 1. Total DOS (top panel) and atomically projected DOS (middle and bottom panels) for $(PbS)_{32}$.

on gold and the probe tip is aligned and is taken to be the reference energy in Eq. (1).

III. RESULTS AND DISCUSSION

Density of states of the quantum dot, $(PbS)_{32}$, obtained at the PW91-DFT level of theory is shown in Figure 1 for which we use a Gaussian broadening factor of 0.2 eV. Here, the upper valence band is composed of the Pb-*s* and Pb-*p* states with the S-*p* states. The peak at about 8 eV below the Fermi energy is associated with the Pb-*s* states. The S-*s* states appear at about 12 eV below the Fermi energy whereas the Pb-*d* states are located at about 17 eV below the Fermi energy of the system. The calculated band gap is about ∼2.0 eV. The nature of the chemical bond in $(PbS)_{32}$ appears to be partially ionic as suggested by the Bader charge analysis[24] indicating a charge transfer of about 0.9 *e* from Pb to S.

The electron transport properties are calculated using the STM-like setup,[22] where $(PbS)_{32}$ is deposited on either Au (001) or Au (110) substrate (Figs. 2 and 3). This choice then allows us to examine the role of substrate in determining the tunneling characteristics of $(PbS)_{32}$. The supercell is chosen in such a way that ensures the least mismatch of the lattice of $(PbS)_{32}$ with that of the Au (001) or (110) substrates (see

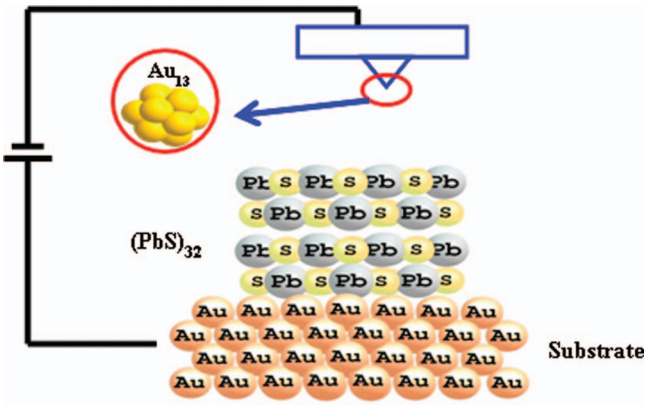

FIG. 2. A schematic illustration of the STM-like setup for $(PbS)_{32}$ deposited on the Au substrate.

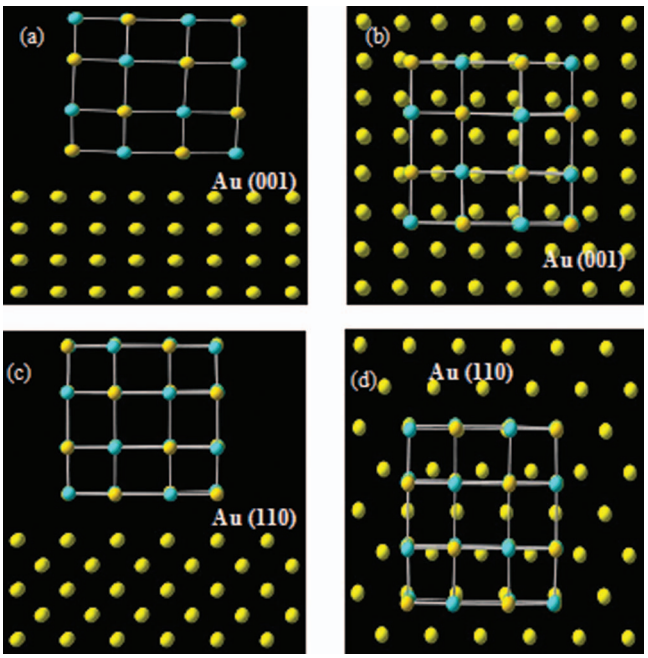

FIG. 3. The side and top views: (a) and (b) $(PbS)_{32}$/Au(001), (c) and (d) $(PbS)_{32}$/Au(110).

Figs. 3(b) and 3(d)). A four-layer slab with 32 atoms per layer is used to simulate the Au (001) substrate (Fig. 3(a)), while a five-layer slab with 24 atoms per layer is used to simulate the Au (110) substrate (Fig. 3(c)). The *xy* dimensions of the supercell are 16.7 × 16.7 Å^2 and 16.7 × 17.7 Å^2 for $(PbS)_{32}$/Au (001) and $(PbS)_{32}$/Au (110), respectively. In addition, a vacuum of 15 Å is added along the z-direction. Such a large supercell is expected to eliminate the interactions among neighboring images in the simulation model. The equilibrium distance between the lower facet of $(PbS)_{32}$ and the Au substrate is calculated to be 2.8 Å, which was obtained by calculating the total energy of the combined system while varying the distance (see Fig. S1 in the supplementary material).[25]

In the setup used for a typical STM experiment (Fig. 2), the probe tip is separated from the quantum dot by a vacuum barrier of 5 Å. The cap configuration of the tip is modeled by a 13-atom Au cluster. The work function of $(PbS)_{32}$ is defined as the energy difference between the vacuum-level potential (calculated from the planar average of the electrostatic potential in the unit cell) and the Fermi energy level of its surface, and is calculated to be ∼4.8 eV.

For the tip, DOS is broadened using Gaussian broadening scheme of width 0.2 eV to take into account the broadening due to its semi-infinite nature, considering that the life time broadening of the electrons of a cluster deposited on a surface is found to be of the order of or greater than 0.2 eV.[26] Note that the Au_{13} cluster is an odd-electron cluster for which we performed the spin-unpolarized electronic structure calculations. The current-voltage characteristics obtained by spin-polarized electronic structure calculations are qualitatively similar to those obtained by spin-unpolarized electronic structure calculations (see Figure S2 in the supplementary material).[25]

The calculated tunneling characteristics of $(PbS)_{32}$ are plotted in Fig. 4 for the bias range of −0.5 V to 0.5 V.

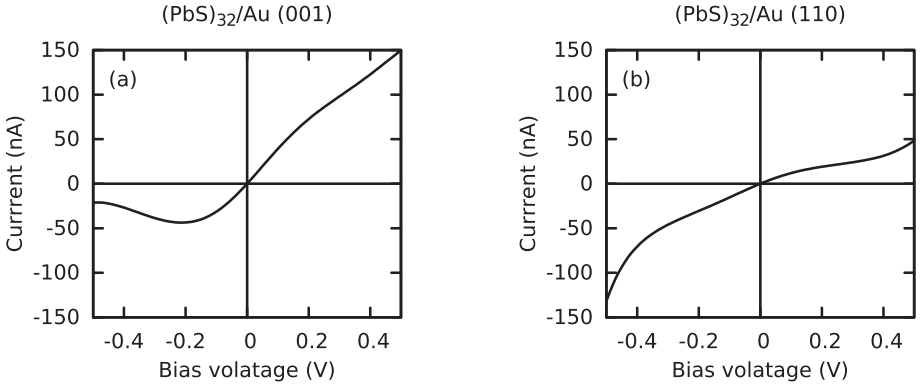

FIG. 4. The current-voltage characteristics of (a) $(PbS)_{32}$/Au (001) and (b) $(PbS)_{32}$/Au (110).

Application of the external bias increases current significantly which is consistent with the observed bright image for $(PbS)_{32}$ in the STM experiments.[19] Most interestingly, the tunneling characteristics are found to be dependent on the nature of the gold substrate. For $(PbS)_{32}$/Au (001), there exists an asymmetric response for the positive and negative values of the external bias as reflected in Fig. 4. This is the renowned molecular diode effect having the ratio of the currents, I(at +0.5 V)/I(at −0.5 V) to be about 6. The predicted behavior brings the promise of application of $(PbS)_{32}$ as a

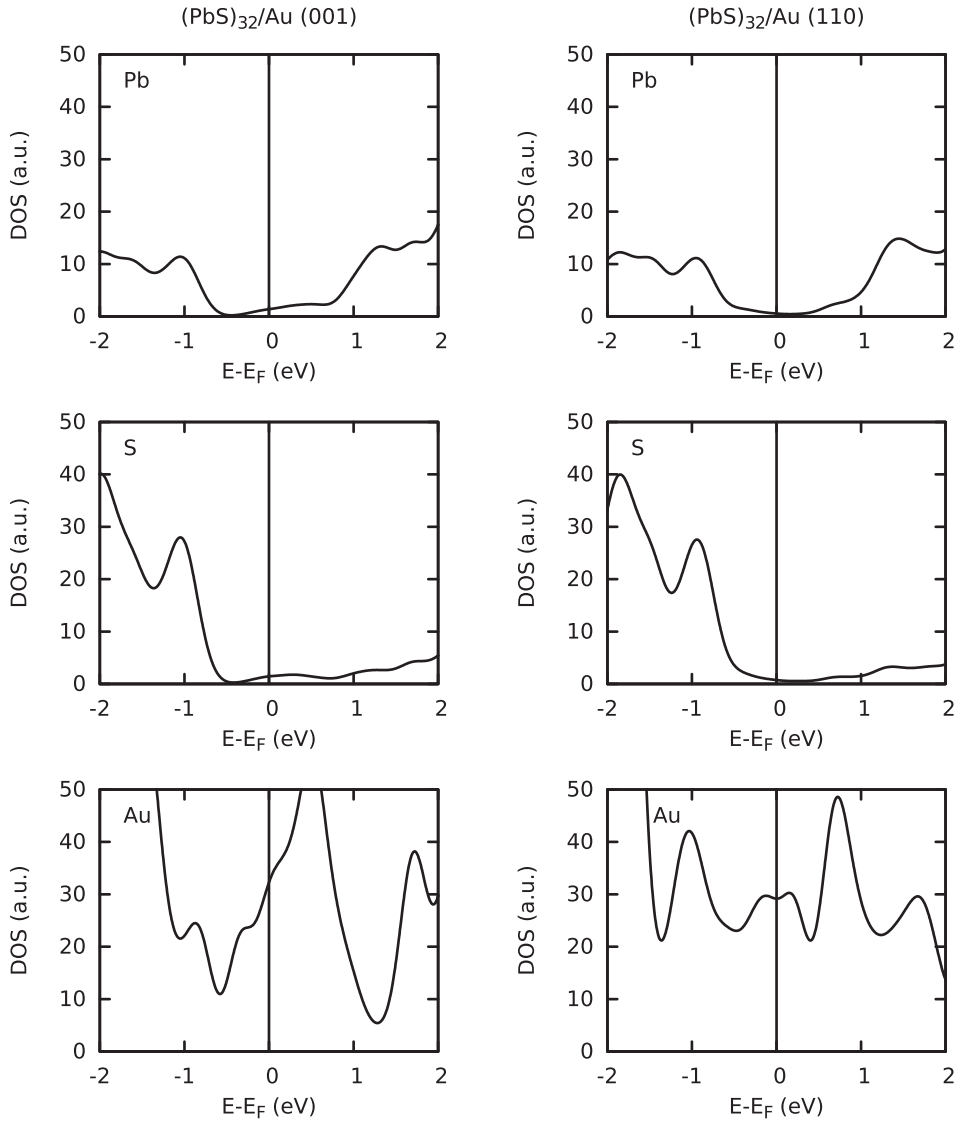

FIG. 5. Atomically projected density of states of $(PbS)_{32}$/Au (001) (on the left) and $(PbS)_{32}$/Au (110) (on the right).

molecular switch.[27,28] On the other hand, the molecular diode effect is less significant for $(PbS)_{32}$/Au(110) for which I(at +0.5 V)/I(at −0.5 V) is calculated to be about 0.4.

In order to further understand the effects of the Au substrate on the tunneling characteristics, DOS of $(PbS)_{32}$/Au (001) and $(PbS)_{32}$/Au (110) are plotted in Figure 5. Considering that the electron tunneling occurs from the tip to $(PbS)_{32}$ under a forward bias, the electrons tunnel from the occupied states of the tip to the unoccupied states of $(PbS)_{32}$. Under the reverse bias, the electron tunneling occurs from the occupied states of $(PbS)_{32}$ to the unoccupied states of the tip. Figure S3 in the supplementary material[25] shows DOS of the cap of the tip simulated by a Au_{13} cluster. Since the tunneling current is directly related to the convolution of the DOS of the tip and the $(PbS)_{32}$ (Eq. (1)), appearance of a finite DOS at the Fermi level is likely to be the cause of the increase in tunneling current with the increase in applied bias. Note that $(PbS)_{32}$ has a band gap of about ∼2.0 eV. Analysis of the atomically projected DOS reveals these additional states at Fermi to be associated with the Au substrate and $(PbS)_{32}$. Nonetheless, due to the differences in the atomic packing of these low-index Au surfaces, the Au (001) surface is better matched with the PbS (001) facet. This leads to a higher degree of hybridization between the Au (001) substrate and $(PbS)_{32}$ for which a broad peak appears from −0.3 eV to 0.7 eV (Fig. 5). The peak has a maximum at about 0.2 eV and drops to almost zero at −0.3 eV, while decreases more slowly towards 0.7 eV. The pronounced diminishing of the peak in the region below Fermi leads to the decrease in the magnitude of tunneling current when the applied bias is less than −0.3 V. In contrast, PDOSs of $(PbS)_{32}$/Au (110) does not show such features yielding continuously increment in tunneling current as one increases the voltage in both positive and negative bias regime.

The location of the hybridized states associated with the interface between $(PbS)_{32}$ and the Au substrate is further confirmed in Figure 6 which shows the enrichment of electrons

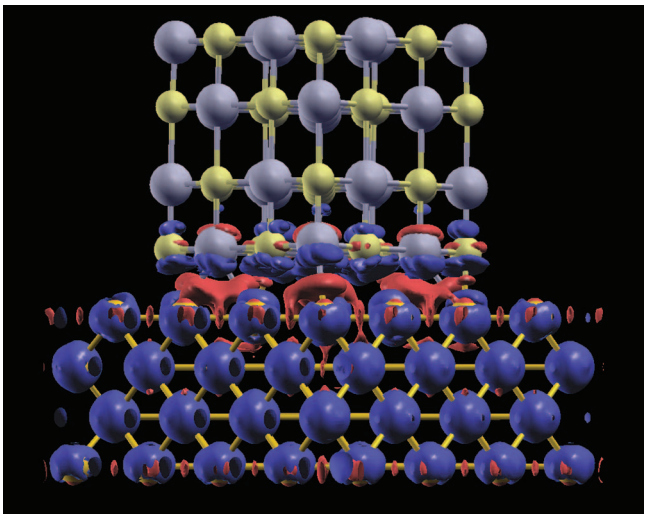

FIG. 6. Difference charge density plot of $(PbS)_{32}$/Au (001). Blue and red represent regions of enhanced and depleted electron density, respectively. Atomic symbols: Pb in gray, S in yellow, and Au in golden yellow. The charge density contours are 1/8th (0.004 e/Å^3) of the maximum value.

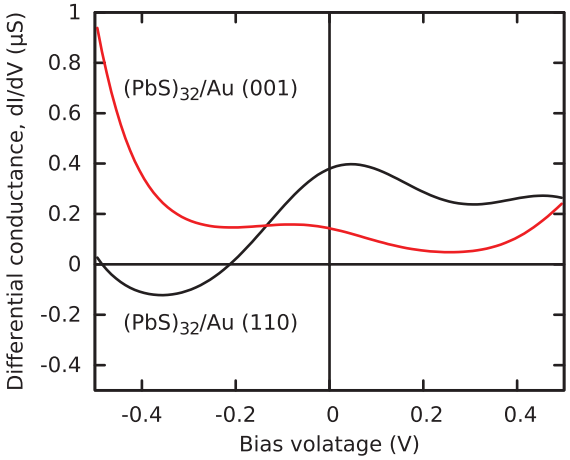

FIG. 7. Differential conductance curve for $(PbS)_{32}$/Au (001) and $(PbS)_{32}$/Au (110).

near Au (001) (blue globes) while the deficit of electrons (red globes) near $(PbS)_{32}$. Furthermore, the band-decomposed charge density plots within the energy range of ±0.2 eV near the Fermi level (see Figs. S4 and S5 in the supplementary material)[25] show that these states are essentially composed of the Au states and *sp* states of Pb and S at the interface. The states below the Fermi energy can be attributed more to the S atoms, while the states above the Fermi energy have a larger contribution from one interface Pb atom sitting on top of an Au atom. This is in line with the observation that in the pristine $(PbS)_{32}$ baby crystal, the top of valence band is primarily composed of S states, while the bottom of the conduction band is composed of Pb states. Furthermore, these states (reflected in the projected density of states of $(PbS)_{32}$ on Au) are not symmetrically distributed around Fermi level, which explains why the tunneling current is also asymmetric and has a diode-like behavior for $(PbS)_{32}$/Au (001).

The distinct states in DOS of a given system can lead to the negative differential resistance (NDR) effect in the STM-like setup. Such an effect is clearly demonstrated for $(PbS)_{32}$/Au (001) in the differential conductance characteristics (Fig. 7), which has a negative value for the bias voltage ranging from −0.3 V to −0.5 V. In this regime, there is a mismatch of the DOS of tip and sample leading to suppression in tunneling at certain bias. It could be followed by the bias voltage for which tunneling is strongly favored. This substrate-dependent feature for $(PbS)_{32}$ could be useful in the photovoltaic applications.

IV. SUMMARY

We have demonstrated that the smallest stable cubic quantum dot of the PbS family, $(PbS)_{32}$ yields a high tunneling current when supported on the Au substrate. Unusual quantum transport properties including the molecular diode-like characteristics and the NDR effect are predicted for $PbS)_{32}$/Au (001). Owing to the hybridization of states associated with $(PbS)_{32}$ and the Au substrate at the interface, finite density of states appears near the Fermi level of the semiconducting system. These hybridized states are the primary

conducting channels for $(PbS)_{32}$ supported on Au. Asymmetric distribution of these states due to the polarity of the material (Pb vs. S) results in the diode-like behavior, while the discrete feature of these electronic states leads to the NDR effect. Therefore, despite the intrinsic gap in bare quantum dot, manipulation of the supporting substrate provides a useful way to tailor the electronic and transport properties of the $(PbS)_{32}$.

ACKNOWLEDGMENTS

S.K.G. acknowledges award of the Fulbright-Nehru Postdoctoral Research Fellowship by United States-India Educational Foundation (USIEF) and Grant No. 1638/FNPDR/2012. Helpful discussions with S. Gowtham are also acknowledged. RAMA and Superior, a high performance computing clusters at Michigan Technological University, were used in obtaining results presented in this paper.

[1]F. W. Wise, Acc. Chem. Res. **33**, 773 (2000).
[2]L. Bakueva, S. Musikhi, M. A. Hines, T.-W. F. Chang, M. Tozolov, G. D. Scholes, and E. H. Sargent, Appl. Phys. Lett. **82**, 2895 (2003).
[3]M. A. Hines and G. D. Scholes, Adv. Mater. **15**, 1844 (2003).
[4]L. Bakueva, I. Gorelikov, S. Musikhin, X. S. Zhao, E. H. Sargent, and E. Kumacheva, Adv. Mater. **16**, 926 (2004).
[5]A. R. Watt, P. Meredith, J. D. Riches, S. Atkinson, and H. Rubinsztein-Dunlop, Curr. Appl. Phys. **4**, 320 (2004).
[6]S. A. McDonald, G. Konstantatos, S. Zhang, P. W. Cyr, E. J. D. Klem, L. Levina, and E. H. Sargent, Nature Mater. **4**, 138 (2005).
[7]J. Nozik, Inorg. Chem. **44**, 6893 (2005).
[8]R. J. Ellingson, M. C. Beard, J. C. Johnson, P. Yu, O. L. Micic, A. J. Nozik, A. Shabaev, and A. L. Efros, Nano Lett. **5**, 865 (2005).
[9]J. J. Peterson and T. D. Krauss, Nano Lett. **6**, 510 (2006).
[10]H. Cao, G. Wang, S. Zhang, and X. Zhang, Nanotechnology **17**, 3280 (2006).
[11]J.-S. Lee, E. V. Shevchenko, and D. V. Talapin, J. Am. Chem. Soc. **130**, 9673 (2008).
[12]E. Istrate, S. Hoogland, V. Sukhovatkin, L. Levina, S. Myskrog, P. W. E. Smith, and E. H. Sargnet, J. Phys. Chem. B **112**, 2757 (2008).
[13]S. Y. Jang, Y. M. Song, H. S. Kim, Y. J. Cho, Y. S. Seo, G. B. Jung, C.-W. Lee, J. Park, M. Jung, J. Kim, B. Kim, J.-G. Kim, and Y.-J. Kim, ACS Nano **4**, 2391 (2010).
[14]S. Mandal and R. Pati, Phys. Rev. B **84**, 115306 (2011).
[15]H. Khan, U. Thupakula, A. Dalui, S. Maji, A. Debangshi, and S. Acharya, J. Phys. Chem. C **117**, 7934 (2013).
[16]S. Wu, H. Zeng, and Z. A. Schelly, Langmuir **21**, 686 (2005).
[17]H. Zeng, Z. A. Schelly, K. Ueno-Noto, and D. S. Marynick, J. Phys. Chem. A **109**, 1616 (2005).
[18]J. He, C. Liu, F. Li, R. Sa, and K. Wu, Chem. Phys. Lett. **457**, 163 (2008).
[19]B. Kiran, A. K. Kandalam, R. Rallabandi, P. Koirala, X. Li, X. Tang, Y. Wang, H. Fairbrother, G. Gantefoer, and K. Bowen, J. Chem. Phys. **136**(2), 024317 (2012).
[20]G. Kresse and J. Furthmuller, Phys. Rev. B **54**(16), 11169 (1996).
[21]J. P. Perdew, J. A. Chevary, S. H. Vosko, K. A. Jackson, M. R. Pederson, D. J. Singh, and C. Fiolhais, Phys. Rev. B **46**, 6671 (1992).
[22]H. He, R. Pandey, R. Pati, and S. P. Karna, Phys. Rev. B **73**(19), 195311 (2006).
[23]J. Tersoff and D. R. Hamann, Phys. Rev. Lett. **50**(25), 1998 (1983).
[24]W. Tang, E. Sanville, and G. Henkelman, J. Phys. Condens. Matter **21**(8), 084204 (2009).
[25]See supplementary material at http://dx.doi.org/10.1063/1.4849136 for supporting figures.
[26]L. Bolotov, N. Uchida, and T. Kanayama, Eur. Phys. J. D **16**(1–3), 271 (2001).
[27]S. Mandal and R. Pati, ACS Nano **6**(4), 3580 (2012).
[28]P. Bedrossian, D. M. Chen, K. Mortensen, and J. A. Golovchenko, Nature (London) **342**(6247), 258 (1989).